Accurate coupled vibration analysis of a piezoelectric array element by the superposition method

Wenxiang Ding, Maxime Bavencoffe, Marc Lethiecq

Accurate Coupled Vibration Analysis of a Piezoelectric Array Element by the Superposition Method

Wenxiang Ding[1*], Maxime Bavencoffe[1], Marc Lethiecq[1]

[1]GREMAN UMR 7347 CNRS, Université de Tours, INSA Centre Val de Loire, 3 Rue de la Chocolaterie, 41000, Blois, France

Abstract

In this paper, the superposition method is extended to obtain analytical solutions for the coupled vibration of a piezoelectric slender bar in a configuration corresponding to a typical ultrasonic linear array transducer element. The problem can be described mathematically by three partial differential equations with electrical and mechanical boundary conditions. To solve this, the vibrations in lateral and thickness directions are referred to as two building blocks. In each building block, the expressions of displacements and electric potential are assumed first based on their symmetry properties and then the induced dynamic responses, such as in-plane stress and electric displacements, are calculated. Finally, the vibration responses of the two building blocks are superimposed to satisfy the boundary conditions using Fourier series expansions. Electrical impedance and mode shapes, represented by the spatial distribution of displacements and electric potential, are calculated analytically and compared with the results of the finite element method. An excellent agreement is observed. The method can be applied to design and optimize piezoelectric array transducers for various applications.

Keywords: coupled vibration, analytical model, superposition method, electrical impedance, piezoelectric array element, finite element method

1. Introduction

As it is well known, the piezoelectric elements in linear array transducers used for ultrasonic imaging are usually in the form of rectangular slender bars, poled along their thickness. The piezoelectric elements can generally be considered as two-dimensional (2D) structures since the length is much larger than the width and the thickness. Moreover, if the width is much larger or smaller than the thickness, then a simple one-

* Corresponding author.
Email address: wenxiang.ding@insa-cvl.fr (Wenxiang Ding), maxime.bavencoffe@insa-cvl.fr (Maxime Bavencoffe), marc.lethiecq@insa-cvl.fr (Marc Lethiecq).

dimensional (1D) model, dominated by either width or thickness vibration mode, can be used to characterize the behavior of the transducer [1]. Similarly, various vibration modes in piezoelectric ceramics have been modelled by making 1D approximations of different geometrical shapes of samples. Results are summarized in some textbooks [2,3] and standards [4].

The 1D theory usually considers only the uncoupled motion of the sample in a specific direction. It gives a good prediction of the basic behavior of the transducer and has been widely applied to transducer design and manufacture [5–7]. However, due to the piezoelectric effect and Poisson's ratio, coupling effects are involved in the vibration modes and the 1D theory is no longer applicable to describe mode interactions. In order to address this, a 2D or three-dimensional (3D) model is needed. The vibration of a piezoelectric element can be described mathematically by a system of three (for a 2D model) or four (for a 3D model) coupled partial differential equations (PDEs). Among these equations, one relates to the electric field and the other two or three to the mechanical field. The biggest difficulties in solving these equations lie in finding the right expressions for the functions of unknown variables, i.e. mechanical displacements and electric potential in this case. They are generally functions of all spatial coordinates and time and need to satisfy the mechanical and electrical boundary conditions. Since the exact solution to this problem is very difficult to obtain, approximation methods are usually required. One way to reduce the complexity is to use decoupled field functions. Brissaud [8,9] proposed an approximated 3D model wherein the displacement along each propagation direction is independent, only related to the corresponding coordinate, and the electrical quantities, i.e. electric field and electric displacement, in non-polarized directions are assumed to be zero. Recently, Brissaud [10] developed a model to characterize the coupling between shear and longitudinal modes inside rectangular elements. Pappalardo *et al.* [11,12] adopted two orthogonal functions to represent displacements. Although the expressions combine a sine and a cosine function, they are still only related to the corresponding coordinate. Besides, the piezoelectric constant e_{31} has to be omitted so as to satisfy the electrical boundary condition. Another kind of approximate solution was presented by Tiersten [13] where a set of solutions was combined with undetermined coefficients, one from the solution of the thickness vibration of a plate and the other one from that of 2D standing waves in an elastic plate. The boundary conditions were satisfied by the method of least squares. The undesirable feature of this method is the non-uniqueness of the solution. Moojoon [14] also presented similar expressions of displacements for the coupled equations. However, the derivation neglected shear vibration and the coupling from electric field was not considered in the mechanical field equations. In addition, high order of approximation methods by expanding the displacements and electric potential in cosine or power series were also developed by Lee [15,16] and Li [17]. The calculated dispersion curves, i.e.

frequency vs dimension ratios, gave a good prediction.

In fact, the coupling effect between vibration modes in elastic materials has been given attention for decades, some studies dating back to the 1930s [18]. The theoretical problem of conducting a free vibration analysis of a completely free rectangular plate has a history of almost a century [19]. Various quasi-exact approaches have been developed for the vibration of thin plates with different kinds of boundary conditions, such as Rayleigh-Ritz [20–23] and Galerkin method [24,25]. For a comprehensive review of these methods, one can refer to [26–28]. The superposition method was first proposed by Gorman and has been successfully employed to solve various vibration problems of elastic structures [19,29–31]. The method seeks an analytical solution for each of the vibrations in lateral and thickness directions, considered as two building blocks, and then superimposes them to satisfy the boundary conditions. Recently, Daeseung *et al.* [32] tried to extend the superposition method to analyze the coupled vibration of a piezoelectric element. However, they only considered the two coupled differential equations of mechanical field while the third one of electric field was missed out.

Approximate methods mentioned above are either based on uncoupled field functions or developed without the consideration of shear vibrations or electric field coupling. For all of them, the constitutive equations are not satisfied in some way. In the present work, the superposition method is extended to solve the coupled vibration problem of a piezoelectric array element, which to our knowledge had never been realized successfully. This analytical model can be applied to several types of piezoelectric materials whose symmetry classes belong to orthorhombic 2mm, tetragonal 4mm and hexagonal 6mm due to the similarities in their elastic, piezoelectric and dielectric tensors [33]. The vibrations in lateral and thickness directions are separated and referred to as two building blocks. In each building block, appropriate expressions of displacements and electric potential are given based on their symmetry properties. By inserting them into the coupled differential equations, the induced dynamic responses are obtained. Solutions from the two building blocks are then superimposed to satisfy the boundary conditions by means of Fourier series expansions. The results are compared with those obtained by the finite element (FE) method and discussed.

2. Mathematical Formulation

The derivation of the analytical solutions focuses on transversely isotropic materials which exhibit hexagonal 6mm symmetry with five elastic, three piezoelectric and two dielectric constants. Fig. 1 shows the coordinate system and dimensions for a typical

piezoelectric slender bar such as those used as ultrasonic array element. The poling direction is parallel to z axis. Since the length of the element is much larger than the thickness and the width ($L \gg H > W$), the strain along y axis can be considered as constant, in which case the problem can be reduced to a 2D one as shown in Fig. 1(b).

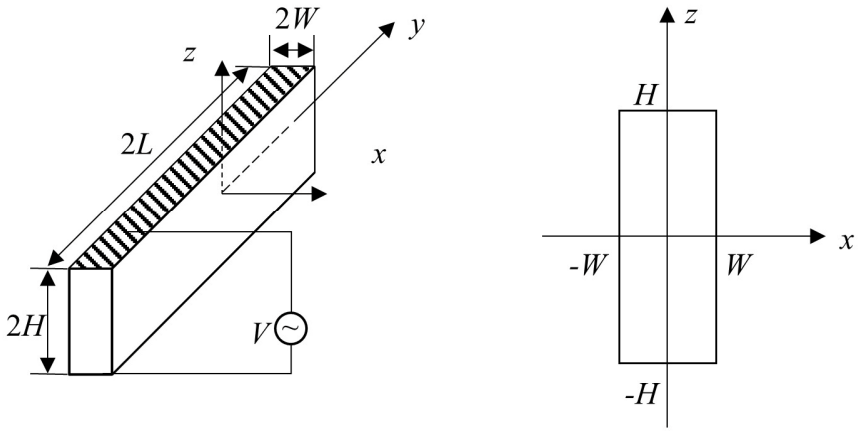

(a) (b)

Fig. 1. Schematic representation of the piezoelectric slender bar. (a) three-dimensional (3D) problem; (b) two-dimensional (2D) problem.

The constitutive equations of a piezoelectric element can be expressed as [33]

$$\begin{aligned} T_\alpha &= c_{\alpha\beta}^E S_\beta - e_{i\alpha} E_i \\ D_i &= \varepsilon_{ij}^S E_j + e_{i\alpha} S_\alpha \end{aligned} \quad i, j = 1,2,3 \text{ and } \alpha, \beta = 1,...,6 \tag{1}$$

where $c_{\alpha\beta}^E$ are the elastic stiffness constants under constant electric field, $e_{i\alpha}$ are the piezoelectric constants, ε_{ij}^S are the dielectric constants under constant strain, T_α, S_β, E_i and D_i are the stress, strain, electric field and electric displacement, respectively.

Since the length of the piezoelectric slender bar is much larger than the thickness and width, it satisfies plane strain condition in y axis, thus $S_2 = S_4 = S_6 = 0$. The interaction between y axis and xz plane can be omitted. Therefore, electric field E_2 and electric displacement D_2 are equal to zero. With these hypotheses, Eq. (1) can be simplified and rewritten as follows

$$\begin{aligned} T_1 &= c_{11}^E S_1 + c_{13}^E S_3 - e_{31} E_3 \\ T_3 &= c_{13}^E S_1 + c_{33}^E S_3 - e_{33} E_3 \\ T_5 &= c_{55}^E S_5 - e_{15} E_1 \\ D_1 &= e_{15} S_5 + \varepsilon_{11}^S E_1 \\ D_3 &= e_{31} S_1 + e_{33} S_3 + \varepsilon_{33}^S E_3 \end{aligned} \tag{2}$$

The strains and displacements are related by

$$S_1 = \frac{\partial u}{\partial x}, S_3 = \frac{\partial w}{\partial z}, S_5 = \frac{\partial u}{\partial z} + \frac{\partial w}{\partial x} \tag{3}$$

The electric fields are related to the electric potential by

$$E_1 = -\frac{\partial \varphi}{\partial x}, E_3 = -\frac{\partial \varphi}{\partial z} \tag{4}$$

The equations of motion and Maxwell's equation for electrostatic field are

$$\begin{aligned} &\frac{\partial T_1}{\partial x} + \frac{\partial T_5}{\partial z} = \rho \frac{\partial^2 u}{\partial t^2} \\ &\frac{\partial T_5}{\partial x} + \frac{\partial T_3}{\partial z} = \rho \frac{\partial^2 w}{\partial t^2} \\ &\frac{\partial D_1}{\partial x} + \frac{\partial D_3}{\partial z} = 0 \end{aligned} \tag{5}$$

Substituting Eqs. (2)-(4) into Eq. (5) yields three coupled differential equations

$$\begin{aligned} &c_{11}^E \frac{\partial^2 u}{\partial x^2} + \left(c_{13}^E + c_{55}^E\right) \frac{\partial^2 w}{\partial z \partial x} + c_{55}^E \frac{\partial^2 u}{\partial z^2} + \left(e_{31} + e_{15}\right) \frac{\partial^2 \varphi}{\partial z \partial x} = \rho \frac{\partial^2 u}{\partial t^2} \\ &c_{33}^E \frac{\partial^2 w}{\partial z^2} + \left(c_{13}^E + c_{55}^E\right) \frac{\partial^2 u}{\partial z \partial x} + c_{55}^E \frac{\partial^2 w}{\partial x^2} + e_{33} \frac{\partial^2 \varphi}{\partial z^2} + e_{15} \frac{\partial^2 \varphi}{\partial x^2} = \rho \frac{\partial^2 w}{\partial t^2} \\ &e_{15} \frac{\partial^2 w}{\partial x^2} + \left(e_{15} + e_{31}\right) \frac{\partial^2 u}{\partial z \partial x} + e_{33} \frac{\partial^2 w}{\partial z^2} - \varepsilon_{11}^S \frac{\partial^2 \varphi}{\partial x^2} - \varepsilon_{33}^S \frac{\partial^2 \varphi}{\partial x^2} = 0 \end{aligned} \tag{6}$$

where the three variables are u, w and φ. The former two are respectively the displacements along x and z axes, and the last one is the electric potential.

Because there are no electrodes on the lateral surfaces, their electric displacement is equal to zero. In addition, the piezoelectric element is stress free and an AC-voltage is applied on the electrodes, therefore, the electrical and mechanical boundary conditions can be expressed as

$$\begin{aligned} &T_1 = T_5 = D_1 = 0 \qquad \text{at} \quad x = \pm W \\ &T_3 = T_5 = 0, \varphi = \pm \varphi_0 \, \mathrm{e}^{\mathrm{j}\omega t} \quad \text{at} \quad z = \pm H \end{aligned} \tag{7}$$

The major difficulty in solving the problem is to find suitable expressions of variables which simultaneously satisfy the coupled equations in Eq. (6) and the mechanical and electrical boundary conditions in Eq. (7). Before exploring solutions to the coupled equations described above, it is necessary to investigate the symmetry properties of the displacements and electric potential inside the element. In Ref.[29], three mode families are proposed to represent the final solutions. They are defined as symmetric-symmetric, antisymmetric-antisymmetric and symmetric-antisymmetric modes. Actually, the vibration of a piezoelectric element is a special form of "free" vibration: when an AC-voltage is applied on the metallized electrode, a symmetric "force" is applied on the top and bottom surface simultaneously due to the piezoelectric effect. Even if this force is not a traditional mechanical volume or surface force, the electric boundary condition constrains the vibration of the structure to only symmetric-

symmetric vibrations. Therefore, the symmetry properties of the in-plane displacements and electric potential can be summarized as follows

$$\begin{aligned} u(x,z) &= u(x,-z) \quad \text{and} \quad u(x,z) = -u(-x,z) \\ w(x,z) &= -w(x,-z) \quad \text{and} \quad w(x,z) = w(-x,z) \\ \varphi(x,z) &= -\varphi(x,-z) \quad \text{and} \quad \varphi(x,z) = \varphi(-x,z) \end{aligned} \tag{8}$$

where the displacement $u(x,z)$ is an even function versus z coordinate but an odd function versus x coordinate; the displacement $w(x,z)$ and the electric potential $\varphi(x,z)$ are odd functions versus z coordinate but even functions versus x coordinate.

2.1 General solution for displacement and electric potential

Due to the symmetry property, the study is limited to a quarter of the element, as shown in Fig. 2(a). Two pairs of small circles indicate the symmetry condition along each side. In order to establish a correct solution satisfying the boundary condition, the model is divided in two building blocks as shown schematically in Fig. 2(b). The way to perform the superposition is slightly different than Gorman's one [29,30]. In Gorman's method, a set of two linear equations has to be solved first to obtain the coefficients of displacements from those of edge driving forces. In the present work, this step is avoided. The coefficients of the displacements and electric potential are used directly in the derivation process and in the assembly of final nonhomogeneous linear system. This method is easier to implement especially when there are more than two variables.

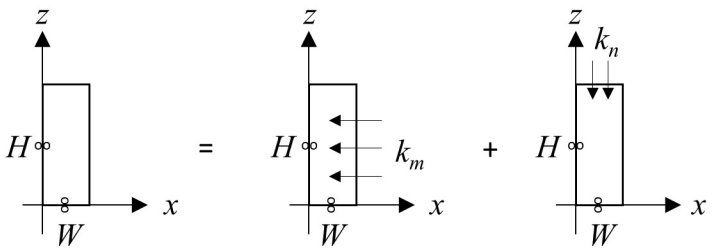

(a) (b)

Fig. 2. Schematic representation of a quarter of the slender bar (a) and two divided building blocks (b) for symmetric-symmetric mode analysis.

Let's now consider the first building block on the left of Fig. 2(b), where only the lateral vibration is induced. Combine with their symmetry properties shown in Eq. (8), the displacements and electric potential are expressed as follows in terms of a Levy-type solution

$$
\begin{aligned}
&u_m(x,z) = U_m(z)\sin(k_m x)\\
&w_m(x,z) = W_m(z)\cos(k_m x) \quad k_m = (2m-1)\frac{\pi}{2W} \text{ and } (m = 1,2,...,+\infty)\\
&\varphi_m(x,z) = \psi_m(z)\cos(k_m x)
\end{aligned} \tag{9}
$$

where k_m is the wavenumber in the lateral direction. For simplicity, the time component $e^{j\omega t}$ is omitted. By substituting Eq. (9) into the coupled equations Eq. (6), we obtain

$$c_{55}^E U_m''(z) + \left(\rho\omega^2 - c_{11}^E k_m^2\right) U_m(z) - \left(c_{13}^E + c_{55}^E\right) k_m W_m'(z) - \left(e_{31} + e_{15}\right) k_m \psi_m'(z) = 0 \tag{10a}$$

$$c_{33}^E W_m''(z) + \left(\rho\omega^2 - c_{55}^E k_m^2\right) W_m(z) + \left(c_{13}^E + c_{55}^E\right) k_m U_m'(z) + e_{33}\psi_m''(z) - e_{15} k_m^2 \psi_m(z) = 0 \tag{10b}$$

$$e_{33} W_m''(z) - e_{15} k_m^2 W_m(z) + \left(e_{31} + e_{15}\right) k_m U_m'(z) - \varepsilon_{33}^S \psi_m''(z) + \varepsilon_{11}^S k_m^2 \psi_m(z) = 0 \tag{10c}$$

where the single apostrophe implies differentiation with respect to the variable z once, double apostrophe implies twice, and so on.

From Eqs. (10b) and (10c) , we can see that the quantities $\psi_m(z)$ and $\psi_m''(z)$ can be expressed in terms of $W_m''(z)$, $W_m(z)$ and $U_m'(z)$. Combine with Eq. (10a), we have a set of equations without the variable $\psi_m(z)$ and its derivatives

$$a_{m1} U_m''(z) + a_{m2} U_m(z) + a_{m3} W_m'''(z) + a_{m4} W_m'(z) = 0 \tag{11a}$$

$$b_{m1} U_m'''(z) + b_{m2} U_m'(z) + b_{m3} W_m''(z) + b_{m4} W_m(z) = 0 \tag{11b}$$

where the coefficients a_{mi} and b_{mi} (i = 1,2,3,4) are constants expressed in terms of material properties, ω and k_m. They are defined in the Appendix (Eq. (A. 1)).

Differentiating Eq. (11b) once with respect to z, we can obtain $W_m'''(z)$ and $W_m'(z)$ in terms of $U_m^{iv}(z)$, $U_m''(z)$ and $U_m(z)$. Let $U_m'''(z)$ be equal to $U_m'(z)$ differentiating twice with respect to z, then we obtain the following sixth order homogeneous differential equation involving only the quantity $U_m(z)$

$$U_m^{vi}(z) + b_1 U_m^{iv}(z) + c_1 U_m''(z) + d_1 U_m(z) = 0 \tag{12}$$

where

$$b_1 = \left(a_{m3}b_{m2} + a_{m4}b_{m1} - a_{m1}b_{m3}\right)/a_{m3}b_{m1}, c_1 = \left(a_{m4}b_{m2} - a_{m1}b_{m4} - a_{m2}b_{m3}\right)/a_{m3}b_{m1}$$
$$d_1 = -a_{m2}b_{m4}/a_{m3}b_{m1}$$

From Eq. (11b), we are also able to express the quantity $W_m(z)$ in terms of $U_m(z)$ and its derivatives

$$W_m(z) = b_2 U_m^v(z) + c_2 U_m'''(z) + d_2 U_m'(z) \tag{13}$$

Finally, turning back to Eq. (10a), the quantity $\psi_m(z)$ is given by

$$\psi_m(z) = b_3 U_m^v(z) + c_3 U_m'''(z) + d_3 U_m'(z) \tag{14}$$

where the coefficients b_2, c_2, d_2, b_3, c_3 and d_3 are given in the Appendix (Eq. (A. 2)).

It is clear that the quantity $W_m(z)$ and $\psi_m(z)$ can be expressed by $U_m(z)$, which satisfies the sixth order homogeneous differential equation Eq. (12). After substituting the exponential function $e^{\lambda z}$ into Eq. (12), its characteristic equation is obtained

$$\lambda^6 + b_1\lambda^4 + c_1\lambda^2 + d_1 = 0 \tag{15}$$

The three roots with respect to λ^2 are given by the roots of general cubic equation [34,35]. Roots of the characteristic equation are composed of three sets of square roots, denoted as

$$\lambda_i = \pm k_{mi} \quad (i = 1,2,3) \tag{16}$$

In the present work, we do not classify the different cases of the roots as in Gorman's method [29]. Whether they are real, imaginary, or complex, for the sake of generalization, they are all considered complex. This helps reduce the burden of derivation of the analytical solutions by transferring much of the trivial work to a computer.

The general solution for Eq. (12), while satisfying the condition of an even function versus z coordinate, is therefore written as follows

$$U_m(z) = \sum_{i=1}^{3} U_{mi} \cosh(k_{mi} z) \tag{17}$$

where U_{mi} are arbitrary constants.

Substituting Eq. (17) into Eqs. (13) and (14), the following expressions of the other two variables are obtained

$$\begin{aligned} W_m(z) &= \sum_{i=1}^{3} B_{mi} U_{mi} \sinh(k_{mi} z) \\ \psi_m(z) &= \sum_{i=1}^{3} C_{mi} U_{mi} \sinh(k_{mi} z) \end{aligned} \tag{18}$$

where

$$B_{mi} = b_2 k_{mi}^5 + c_2 k_{mi}^3 + d_2 k_{mi}, \quad C_{mi} = b_3 k_{mi}^5 + c_3 k_{mi}^3 + d_3 k_{mi}$$

Now let's turn to the second building block on the right of Fig. 2(b). It differs from the first block only in that the thickness vibration is induced in this block. The displacements and electric potential are expressed as follows

$$\begin{aligned} u_n(x,z) &= U_n(x)\cos(k_n z) \\ w_n(x,z) &= W_n(x)\sin(k_n z) \quad k_n = (2n-1)\frac{\pi}{2H} \text{ and } (n = 1,2,...,+\infty) \\ \varphi_n(x,z) &= \psi_n(x)\sin(k_n z) \end{aligned} \tag{19}$$

Now, following the same procedure as above, the solutions of the second building block can be obtained. There is no need to give the whole derivation here. To avoid

confusion, the symbol *m* is replaced by symbol *n*.

Substituting Eq. (19) into Eq. (6), equations similar to Eq.(10) are obtained

$$c_{11}^{E}U_n''(x)+\left(\rho\omega^2-c_{55}^{E}k_n^2\right)U_n(x)+\left(c_{13}^{E}+c_{55}^{E}\right)k_nW_n'(x)+\left(e_{31}+e_{15}\right)k_n\psi_n'(x)=0 \tag{20a}$$

$$-\left(c_{13}^{E}+c_{55}^{E}\right)k_nU_n'(x)+c_{55}^{E}W_n''(x)+\left(\rho\omega^2-c_{33}^{E}k_n^2\right)W_n(x)+e_{15}\psi_n''(x)-e_{33}k_n^2\psi_n(x)=0 \tag{20b}$$

$$-\left(e_{31}+e_{15}\right)k_nU_n'(x)+e_{15}W_n''(x)-e_{33}k_n^2W_n(x)-\varepsilon_{11}^{S}\psi_n''(x)+\varepsilon_{33}^{S}k_n^2\psi_n(x)=0 \tag{20c}$$

where the single apostrophe here implies differentiation with respect to the variable *x* once, double apostrophe implies twice, and so on.

Except for the symbol *m* being replaced, expressions after Eq. (11) are exactly the same until we obtain all the solutions of $W_n(z)$, $U_n(z)$ and $\psi_n(z)$

$$\begin{aligned} U_n(x)&=\sum_{i=1}^{3}U_{ni}\sinh\left(k_{ni}x\right)\\ W_n(x)&=\sum_{i=1}^{3}U_{ni}B_{ni}\cosh\left(k_{ni}x\right)\\ \psi_n(x)&=\sum_{i=1}^{3}U_{ni}C_{ni}\cosh\left(k_{ni}x\right) \end{aligned} \tag{21}$$

where

$$B_{ni}=b_2k_{ni}^5+c_2k_{ni}^3+d_2k_{ni},\quad C_{ni}=b_3k_{ni}^5+c_3k_{ni}^3+d_3k_{ni}$$

The expressions and coefficients corresponding to the second building block are detailed in the Appendix (Eq. (A. 3)). Note that we make no distinction between b_i, c_i, d_i (i = 1,2,3) in Eqs. (12)-(14) and (21) for the two building blocks as they are exactly the same except for the corresponding symbol *m* and *n*.

2.2 Assembly procedure of the augmented matrix of the system

The solutions of displacements and electric potential in the two building blocks (Fig. 2) have already been obtained by separating the variables *x* and *z*. They are given in Eq. (9) and Eqs. (17)-(21) and are superimposed to form the final solution

$$
\begin{aligned}
u(x,z) &= U_m(z)\sin(k_m x)+U_n(x)\cos(k_n z)\\
&=\sum_{m=1}^{\infty}\sum_{i=1}^{3}U_{mi}\cosh(k_{mi}z)\sin(k_m x)+\sum_{n=1}^{\infty}\sum_{i=1}^{3}U_{ni}\sinh(k_{ni}x)\cos(k_n z)\\
w(x,z) &= W_m(z)\cos(k_m x)+W_n(x)\sin(k_n z)\\
&=\sum_{m=1}^{\infty}\sum_{i=1}^{3}U_{mi}B_{mi}\sinh(k_{mi}z)\cos(k_m x)+\sum_{n=1}^{\infty}\sum_{i=1}^{3}U_{ni}B_{ni}\cosh(k_{ni}x)\sin(k_n z)\\
\varphi(x,z) &= \psi_m(z)\cos(k_m x)+\psi_n(x)\sin(k_n z)\\
&=\sum_{m=1}^{\infty}\sum_{i=1}^{3}U_{mi}C_{mi}\sinh(k_{mi}z)\cos(k_m x)+\sum_{n=1}^{\infty}\sum_{i=1}^{3}U_{ni}C_{ni}\cosh(k_{ni}x)\sin(k_n z)
\end{aligned}
\tag{22}
$$

Substituting the solution Eq. (22) into the boundary condition Eq. (7), a linear system with respect to the unknown coefficients U_{mi} and U_{ni} is obtained. The results may be presented in a concise way as

$$
\begin{aligned}
&\sum_{m=1,}^{\infty}\sum_{i=1}^{3}F_1^{mi}U_{mi}\cos(k_m x)=0 && \text{as} \quad T_3(z=\pm H)=0\\
&\sum_{n=1}^{\infty}\sum_{i=1}^{3}F_1^{ni}U_{ni}\cos(k_n z)=0 && \text{as} \quad T_1(x=\pm W)=0\\
&\sum_{m=1}^{\infty}\sum_{i=1}^{3}\left\{F_2^{mi}U_{mi}+\sum_{n=1}^{\infty}G_2^{ni}U_{ni}\right\}\sin(k_m x)=0 && \text{as} \quad T_5(z=\pm H)=0\\
&\sum_{n=1}^{\infty}\sum_{i=1}^{3}\left\{F_2^{ni}U_{ni}+\sum_{m=1}^{\infty}G_2^{mi}U_{mi}\right\}\sin(k_n z)=0 && \text{as} \quad T_5(x=\pm W)=0\\
&\sum_{m=1}^{\infty}\sum_{i=1}^{3}\left\{F_3^{mi}U_{mi}+\sum_{n=1}^{\infty}G_3^{ni}U_{ni}\right\}\cos(k_m x)=\varphi_0^{mi} && \text{as} \quad \varphi(z=\pm H)=\pm\varphi_0\\
&\sum_{n=1}^{\infty}\sum_{i=1}^{3}\left\{F_3^{ni}U_{ni}+\sum_{m=1}^{\infty}G_3^{mi}U_{mi}\right\}\sin(k_n z)=0 && \text{as} \quad D_1(x=\pm W)=0
\end{aligned}
\tag{23}
$$

where F_j^{mi} and F_j^{ni} (j =1,2,3) can be easily derived from the previous derivation, they are given by

$$
\begin{aligned}
F_1^{mi} &= \left[\left(c_{33}^E B_{mi}+C_{mi}e_{33}\right)k_{mi}+c_{13}^E k_m\right]\cosh(k_{mi}H)\\
F_1^{ni} &= \left[\left(c_{13}^E B_{ni}+C_{ni}e_{31}\right)k_n+c_{11}^E k_{ni}\right]\cosh(k_{ni}W)\\
F_2^{mi} &= \left[\left(-c_{55}^E B_{mi}-e_{15}C_{mi}\right)k_m+c_{55}^E k_{mi}\right]\sinh(k_{mi}H)\\
F_2^{ni} &= \left[\left(c_{55}^E B_{ni}+e_{15}C_{ni}\right)k_{ni}-c_{55}^E k_n\right]\sinh(k_{ni}W)\\
F_3^{mi} &= C_{mi}\sinh(k_{mi}H)\\
F_3^{ni} &= \left[\left(-\varepsilon_{11}^S C_{ni}+e_{15}B_{ni}\right)k_{ni}-e_{15}k_n\right]\sinh(k_{ni}W)
\end{aligned}
$$

and G_j^{mi}, G_j^{ni}, and φ_0^{mi} (j =1,2,3) are obtained using the Projection method [36]

$$G_2^{ni} = 2\left[\left(c_{55}^E B_{ni} + e_{15} C_{ni}\right) k_{ni} - c_{55}^E k_n\right] \sin\left(k_n H\right) \int_0^W \sin(k_m x) \sinh\left(k_{ni} x\right) dx \Big/ W$$

$$G_2^{mi} = 2\left[\left(-c_{55}^E B_{mi} - e_{15} C_{mi}\right) k_m + c_{55}^E k_{mi}\right] \sin\left(k_m W\right) \int_0^H \sinh\left(k_{mi} z\right) \sin\left(k_n z\right) dz \Big/ H$$

$$G_3^{ni} = 2 C_{ni} \sin\left(k_n H\right) \int_0^W \cosh\left(k_{ni} x\right) \cos(k_m x) dx \Big/ W$$

$$G_3^{mi} = 2\left[\left(\varepsilon_{11}^S C_{mi} - e_{15} B_{mi}\right) k_m + e_{15} k_{mi}\right] \sin\left(k_m W\right) \int_0^H \sinh\left(k_{mi} z\right) \sin\left(k_n z\right) dz \Big/ H$$

$$\varphi_0^{mi} = 2\varphi_0 \int_0^W \cos(k_m x) dx \Big/ W$$

One thing to notice in Eq. (23) is that since $\cos\left(k_n H\right)$ and $\cos\left(k_m W\right)$ are equal to zero, the quantities $\partial u_m\left(x,z\right)\big/\partial x$ and $\partial w_m\left(x,z\right)\big/\partial z$ are consequently equal to zero at $x = \pm W$, so do the quantities $\partial u_n\left(x,z\right)\big/\partial x$ and $\partial w_n\left(x,z\right)\big/\partial z$ at $z = \pm H$. This is the reason why $G_1^{mi} = G_1^{ni} = 0$.

Based on the above theory, assuming that the number of terms used for k_m and k_n in the two building blocks are K_1 (m = 1,…,K_1) and K_2 (n = 1,…,K_2), we obtain a nonhomogeneous linear system with $3(K_1+K_2)$ unknown coefficients U_{mi} and U_{ni}. The linear system in matrix notation is given by

$$\mathbf{Ax} = \mathbf{b} \tag{24}$$

where $\mathbf{A}$ is a $3(K_1+K_2)\times3(K_1+K_2)$ coefficient matrix, $\mathbf{x}$ is the unknown variable, and $\mathbf{b}$ is a $3(K_1+K_2)\times1$ vector with K_1 non-zero elements related to φ_0.

For clarity, an example is shown here. K_1 and K_2 are set to 2. The augmented matrix of the system is assembled and depicted schematically in Fig. 3. It corresponds precisely to Eq. (23), as indicated by the boundary conditions on the right. The elements denoted by an asterisk (*) are F_j^{mi} and F_j^{ni}, those denoted by a short solid bar (-) are G_j^{mi}, G_j^{ni} and φ_0^{mi}, and the rest are zero. The linear system has a unique non-trivial solution associated with φ_0. In other words, the solutions of all the unknown coefficients depend on constant φ_0. Once the constant φ_0 is known, the coefficients can be determined.

U_{m1}		U_{n1}		U_{m2}		U_{n2}		U_{m3}		U_{n3}		φ	
1	2	1	2	1	2	1	2	1	2	1	2		
*				*				*					$T_3\ (z = \pm H)$
	*				*				*				
		*				*				*			$T_1\ (x = \pm W)$
			*				*				*		
*		-	-	*		-	-	*		-	-		$T_5\ (z = \pm H)$
	*	-	-		*	-	-		*	-	-		
-	-	*		-	-	*		-	-	*			$T_5\ (x = \pm W)$
-	-		*	-	-		*	-	-		*		

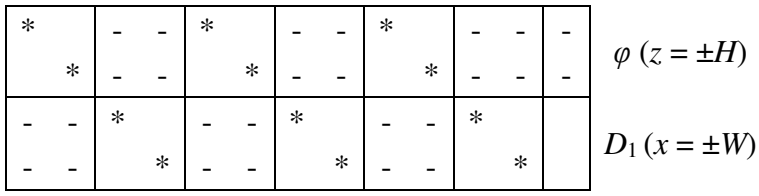

Fig. 3. Schematic representation of assembled augmented matrix of the system (* : F_j^{mi} and F_j^{ni}; -: G_j^{mi}, G_j^{ni}, and φ_0^{mi}).

2.3 Electrical impedance calculation

The electrical impedance of the piezoelectric material is defined as

$$Z=\frac{V}{I} \tag{25}$$

where V is the voltage applied across the electrodes and I is the electric current flowing through the sample.

Since the electric potential on the top and bottom electrode surface is $\pm\varphi_0 \mathrm{e}^{\mathrm{j}\omega t}$, we have

$$V=\int_{-H}^{H} E_3 dz=-\int_{-H}^{H}\frac{\partial\varphi}{\partial z}dz=-2\varphi_0 \mathrm{e}^{\mathrm{j}\omega t} \tag{26}$$

The electric current is defined by the differential of charge versus time. The charge on electrodes can be calculated by integrating the electric displacement density D_3 over the surface. Therefore,

$$I=\frac{\partial}{\partial t}\int_{-L}^{L}\int_{-W}^{W} D_3(x,H,t)dxdy=2\mathrm{j}\omega L\mathrm{e}^{\mathrm{j}\omega t}\int_{-W}^{W} D_3(x,H)dx \tag{27}$$

The general form of $D_3(x,H)$ is given by

$$D_3(x,H)=\sum_{i=1}^{3}\sum_{m=1}^{K_1}\left[\left(e_{33}B_{mi}-\varepsilon_{33}^{S}C_{mi}\right)k_{mi}+e_{31}k_m\right]\cosh(k_{mi}H)\cos(k_m x)U_{mi} \tag{28}$$

After obtaining all the unknown coefficients related to φ_0 in Section 2.2, we can substitute them into Eqs. (25)-(28), then the electrical impedance is determined. This shows that the electrical impedance is only related to the coefficients U_{mi}. The time component $\mathrm{e}^{\mathrm{j}\omega t}$ and the constant φ_0 vanish in the results.

3. Results and Discussion

In order to verify the validity of the analytical model proposed here, the results are compared with those computed by the FE method. The FE analysis is carried out with

COMSOL Multiphysics software. Quadratic Lagrange rectangular elements with nine nodes are used and a frequency domain analysis is performed using N = 5 and N = 18 elements per wavelength for the highest frequency. These two FE configurations are carefully selected to represent a coarse mesh (N = 5, 8×12 elements) and a convergent mesh (N = 18, 16×40 elements) after a mesh convergence study was performed. The validation consists of two parts: the electrical impedance and the mode shape, which is represented by the spatial distribution of the mechanical displacements respectively in the x and z dimensions and the spatial distribution of the electric potential.

The material chosen here is 3203HD, a soft piezoelectric ceramic manufactured by CTS that is widely used in many transducers for its high dielectric constant and high electromechanical coupling coefficient [37]. A rectangular slender bar with dimensions $2L$ = 8 mm, $2H$ = 320 μm and $2W$ = 135 μm, as recommended in [38], is considered. Material properties are listed in Table 1.

Table 1

CTS 3203HD piezoelectric material properties [39]

ρ (kg·m^{-3})	c_{11}^E (GPa)	c_{12}^E (GPa)	c_{13}^E (GPa)	c_{33}^E (GPa)	c_{44}^E (GPa)
7800	107.4	59.3	65.1	98.4	19.1
c_{66}^E (GPa)	e_{31}(C·m^{-2})	e_{33}(C·m^{-2})	e_{15}(C·m^{-2})	ε_{r11}^S	ε_{r33}^S
24.05	-11.03	22.32	19.08	1045	1364

3.1 Electrical impedance

Since the boundary conditions are satisfied in a Fourier series expansion way, the accuracy of this method depends on the number of terms K_1 and K_2 employed for k_m and k_n. Theoretically, any desired degree of accuracy can be achieved by increasing the number of terms. To determine the values of K_1 and K_2, a convergence test for the antiresonance frequency (f_a) is performed. Its variation with the number of terms K_1 = K_2 = K is shown in Fig. 4. The frequency resolution is set at 0.02 MHz. One can see that as the number of terms K increases, the calculated values of f_a converge vertically more or less to an asymptotic value. It should be noted that in the case presented (from 0 MHz to 25 MHz), 6 terms at K are sufficient to allow this asymptotic value to be obtained with good reproducibility.

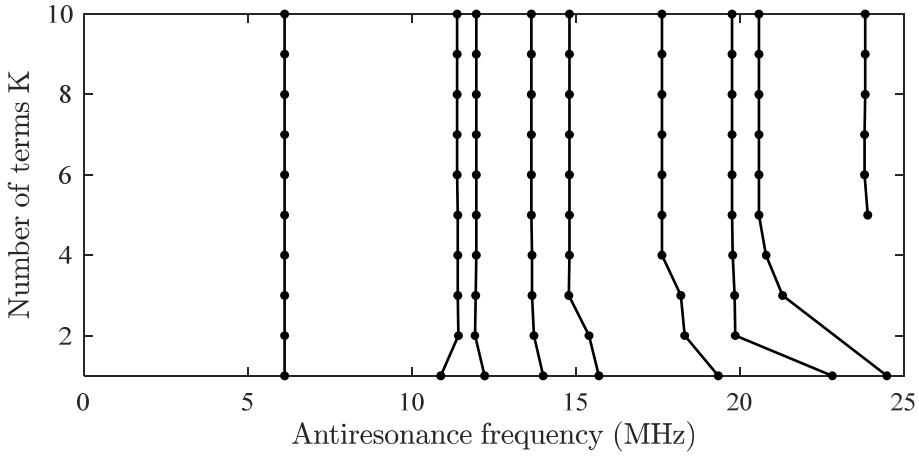

Fig. 4. The variation of antiresonance frequency with the number of terms.

The electrical impedances for three different cases - the number of terms K is equal to 1, 3 and 6 - are shown in Fig. 5 in comparison with the convergent one of FE model (N = 18). As can be seen in Fig. 5 (a), although only one term is used for each vibration mode, the first peaks at around 6.12 MHz are perfectly overlapped. However, in the frequency range higher than 10 MHz, the analytical method can no longer provide sufficient accuracy. The correlation coefficient between the FE model and the analytical one is only 74.31% for this case. As the number of terms increases, the accuracy improves as shown in Fig. 5 (b)-(c) and the correlation coefficient increases to 94.92% and 99.98%, respectively. For a better illustration, the antiresonance frequencies are extracted and relative errors are given in Table 2. The errors are calculated relative to convergent ones of FE simulation when N = 18. An excellent agreement is achieved up to 25 MHz and the maximum discrepancy is around 0.1% when the number of terms equals 6. Based on this, the FE model with N = 18 and analytical model with K1 = K2 = 6 can be considered as having the same precision level. We can also see that coarse mesh gives predictions with larger error at high frequency (> 20 MHz). Table 3 presents the computation times for calculating the electrical impedance. The analytical method shows a great advantage in computational efficiency: the calculation time can be reduced from the FE model's 92.35s to analytical model's 2.6s at the same precision level using Intel (R) Xeon (R) E-2176M CPU, 2.7 GHz with 32 GB memory.

Table 2

The antiresonance frequencies f_a of the piezoelectric element

	FE model		Analytical model		
	N = 5	N = 18	$K_1 = K_2 = 1$	$K_1 = K_2 = 3$	$K_1 = K_2 = 6$
f_{a1} (MHz)	6.12 (0.00%)	6.12	6.12 (0.00%)	6.12 (0.00%)	6.12 (0.00%)
f_{a2} (MHz)	11.40 (0.18%)	11.38	10.88 (4.56%)	11.40 (0.18%)	11.38 (0.00%)
f_{a3} (MHz)	11.96 (0.00%)	11.96	12.22 (2.17%)	11.94 (0.33%)	11.96 (0.00%)
f_{a4} (MHz)	13.64 (0.00%)	13.64	14.00 (2.49%)	13.66 (0.44%)	13.64 (0.00%)

f_{a5} (MHz)	14.84 (0.27%)	14.80	15.70 (6.08%)	14.78 (4.05%)	14.80 (0.00%)
f_{a6} (MHz)	17.76 (0.79%)	17.62	19.34 (9.76%)	18.20 (3.29%)	17.62 (0.00%)
f_{a7} (MHz)	19.80 (0.10%)	19.78	22.82 (15.00%)	19.84 (0.30%)	19.76 (0.10%)
f_{a8} (MHz)	20.82 (1.07%)	20.60	24.48 (18.83%)	21.3 (3.40%)	20.58 (0.10%)
f_{a9} (MHz)	24.52 (2.94%)	23.82	/	/	23.80 (0.08%)

Table 3

Computation times

Model	1250 frequencies calculation time
N = 5 FE model 8×12 elements	31.37s
N = 18 FE model 16×40 elements	92.35s
$K_1 = K_2 = 6$ Analytical model	2.60s

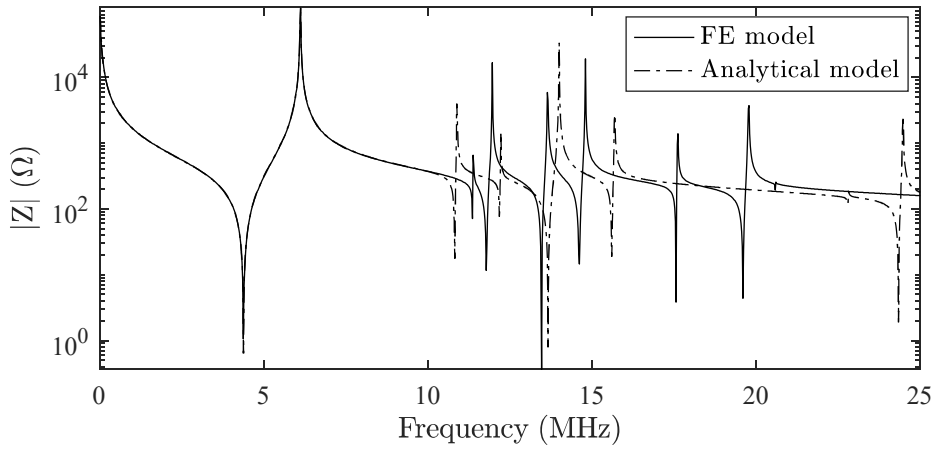

(a)

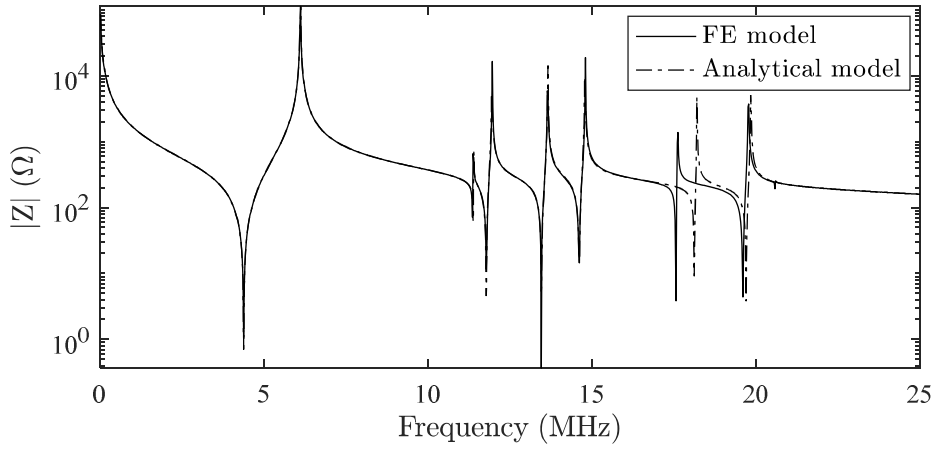

(b)

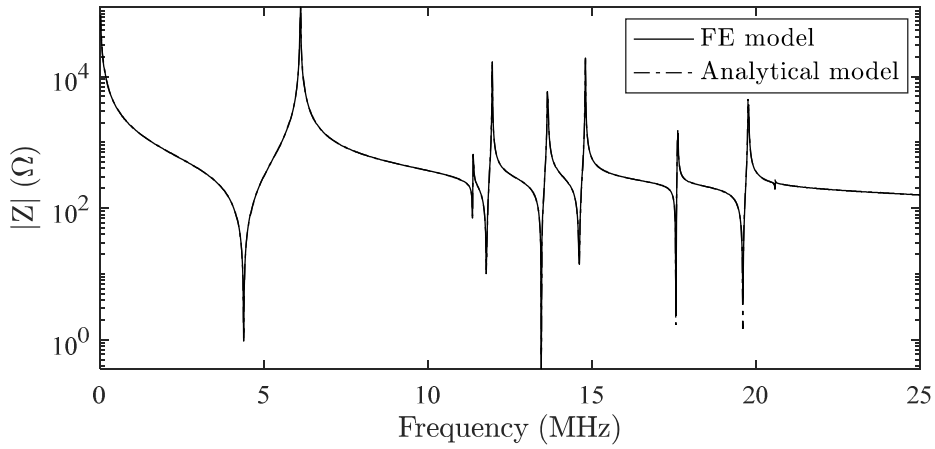

(c)

Fig. 5. The modulus of electrical impedance of the piezoelectric element obtained by using different numbers of terms. (a) $K_1 = K_2 = 1$; (b) $K_1 = K_2 = 3$; (c) $K_1 = K_2 = 6$. Solid lines refer to the results of the FE model and chain dotted lines refer to the results of the present analytical model.

3.2 Mode shape

The mode shapes of displacements u, w and electric potential φ are calculated by substituting the coefficients into Eq. (22). Results at the first antiresonance frequency f_{a1} = 6.12 MHz are obtained using 6 vibration terms and compared to those from the FE model as shown in Fig. 6. The different mode shapes shown in Fig 6 are similar, including not only the spatial variations of curvature, but also the amplitudes. To have a better comparison, the displacements and electric potential along the lateral direction at $z = H/2$ and along the thickness direction at $x = W/2$ are plotted in Fig. 7. An excellent agreement is observed between the results from the FE model and the analytical one. All the correlation coefficients are practically at 100%.

In addition, the symmetry properties mentioned in Eq.(8) can be verified here. That is, the displacement u is an even function versus z but an odd function versus x. The displacement w and electric potential are even functions versus x but odd functions versus z coordinate. We can also find that at frequency f_{a1} = 6.12 MHz, the vibration in thickness direction is predominant as its amplitude w is much bigger than that in lateral direction.

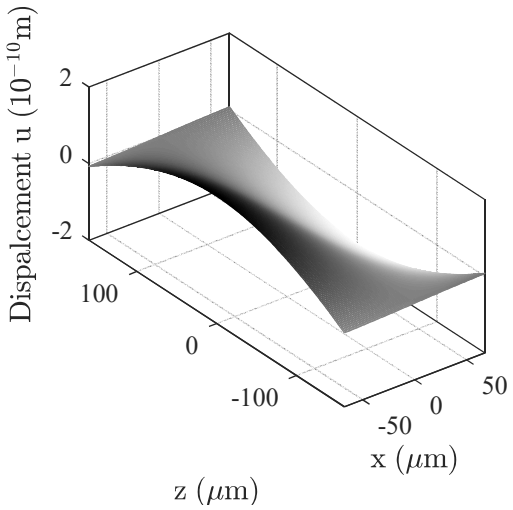
Dispalcement u (10^{-10}m)
2
0
-2
100
0
-100
z (μm)
-50
0
50
x (μm)

(a)

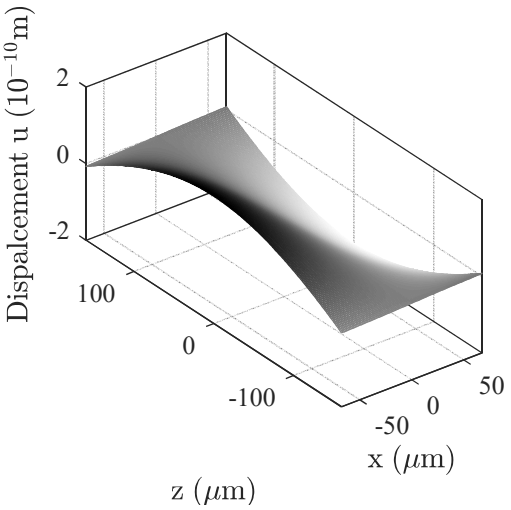
Dispalcement u (10^{-10}m)
2
0
-2
100
0
-100
z (μm)
-50
0
50
x (μm)

(d)

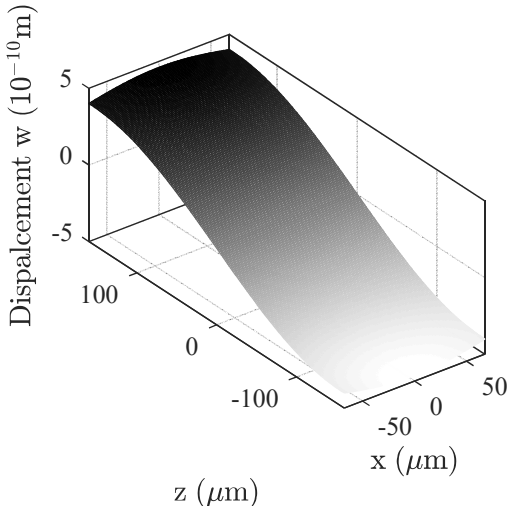
Dispalcement w (10^{-10}m)
5
0
-5
100
0
-100
z (μm)
-50
0
50
x (μm)

(b)

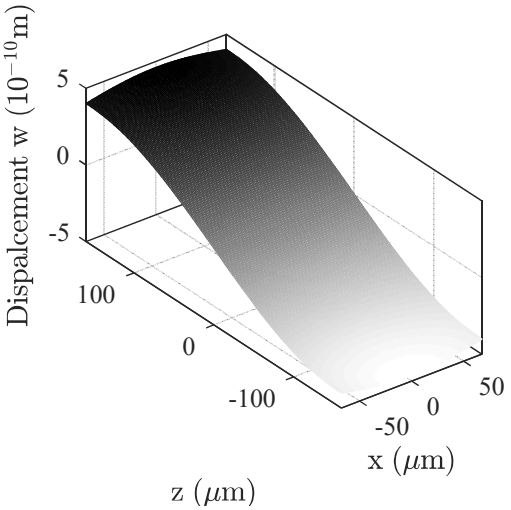
Dispalcement w (10^{-10}m)
5
0
-5
100
0
-100
z (μm)
-50
0
50
x (μm)

(e)

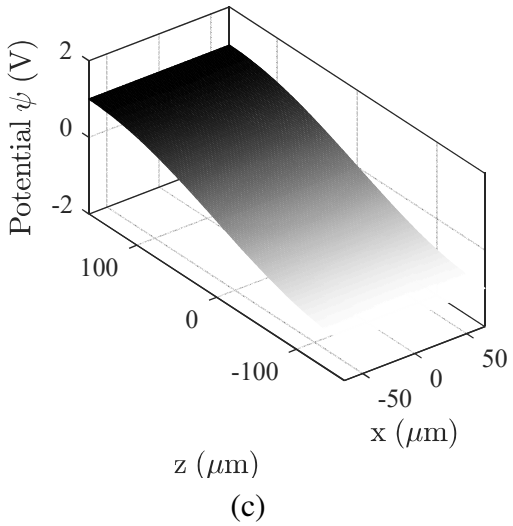
Potential ψ (V)
2
0
-2
100
0
-100
z (μm)
-50
0
50
x (μm)

(c)

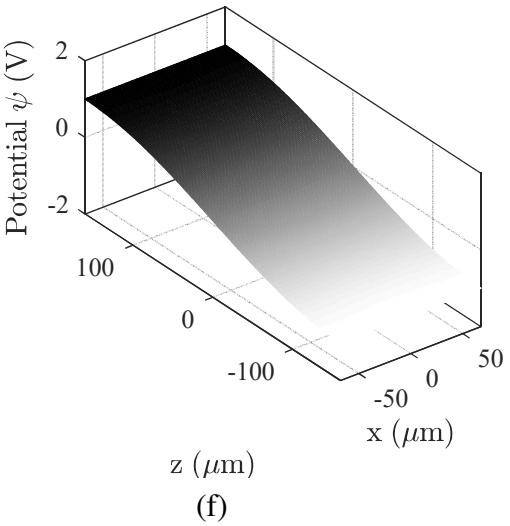
Potential ψ (V)
2
0
-2
100
0
-100
z (μm)
-50
0
50
x (μm)

(f)

Fig. 6. Displacements and electric potential of the piezoelectric element at the first antiresonance frequency (f_{a1} = 6.12 MHz). (a)-(c) indicate results of the FE model; (d)-(f) indicate results of analytical model with $K_1 = K_2 = 6$.

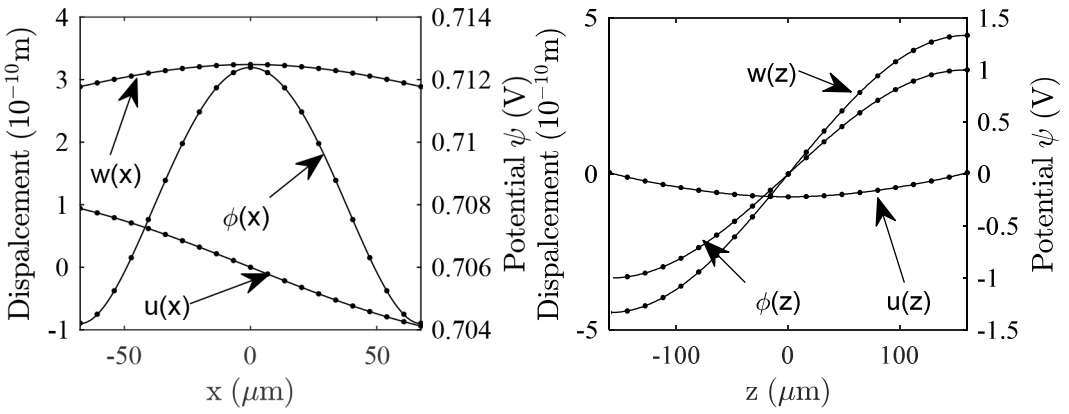

(a) (b)

Fig. 7. Displacements and electric potential distribution at the first antiresonance frequency (f_{a1} = 6.12 MHz). (a) along the lateral direction at $z = H/2$; (b) along the thickness direction at $x = W/2$. Solid lines (–) refer to the results of the FE model and points (•) refer to the results of the present analytical model.

4. Conclusions

In the present work, a two-dimensional analytical model based on the superposition method has been proposed to obtain the coupled dynamic response of piezoelectric array elements. It is derived by dividing the coupled vibration into two building blocks – vibrations in thickness and lateral directions - and superimposing them to form the final solution. The boundary conditions are satisfied via Fourier series expansions.

The proposed analytical model is able to describe the coupling between thickness and width mode in a piezoelectric array element of arbitrary width-to-thickness ratio. A typical size used for ultrasonic array transducer has been selected to demonstrate the effectiveness. The comparison of the electrical impedance and mode shapes calculated by the proposed method and by the FE one shows an excellent agreement. The computational efficiency of the analytical method proposed here has proved to be much higher than that of the FE method (over 30 times faster) at the same level of precision. Another interesting point compared to the FE method is that mesh generation problems are avoided. The model shows a great potential for the design and optimization of ultrasonic array transducers.

Acknowledgement

The work was financially supported by the China Scholarship Council (CSC) through the cooperation program UT-INSA (France).

Appendix

The constants a_{mi} and b_{mi} (i = 1,2,3,4) appearing in Eq. (11) are defined by

$$
\begin{aligned}
a_{m1} &= \frac{\left(c_{13}^{E}+c_{55}^{E}\right)\varepsilon_{33}^{S}+\left(e_{31}+e_{15}\right)e_{33}}{\left(e_{15}\varepsilon_{33}^{S}-e_{33}\varepsilon_{11}^{S}\right)k_m}-\frac{c_{55}^{E}}{\left(e_{31}+e_{15}\right)k_m} \\
a_{m2} &= \frac{c_{11}^{E}k_m}{e_{31}+e_{15}}-\frac{\omega^2\rho}{\left(e_{31}+e_{15}\right)k_m} \\
a_{m3} &= \frac{c_{33}^{E}\varepsilon_{33}^{S}+e_{33}^{2}}{k_m^{2}\left(e_{15}\varepsilon_{33}^{S}-e_{33}\varepsilon_{11}^{S}\right)} \\
a_{m4} &= \frac{c_{55}^{E}+c_{13}^{E}}{e_{31}+e_{15}}-\frac{e_{15}e_{33}}{e_{15}\varepsilon_{33}^{S}-e_{33}\varepsilon_{11}^{S}}+\frac{\left(\rho\omega^2-c_{55}^{E}k_m^{2}\right)\varepsilon_{33}^{S}}{\left(e_{15}\varepsilon_{33}^{S}-e_{33}\varepsilon_{11}^{S}\right)k_m^{2}} \\
b_{m1} &= \frac{e_{33}c_{55}^{E}}{\left(e_{31}+e_{15}\right)k_m} \\
b_{m2} &= \left(-\frac{e_{33}c_{11}^{E}}{e_{31}+e_{15}}-\frac{\left(c_{55}^{E}+c_{13}^{E}\right)e_{33}\varepsilon_{11}^{S}+\left(e_{31}+e_{15}\right)e_{15}e_{33}}{e_{15}\varepsilon_{33}^{S}-e_{33}\varepsilon_{11}^{S}}\right)k_m+\frac{e_{33}\rho\omega^2}{\left(e_{31}+e_{15}\right)k_m} \\
b_{m3} &= c_{33}^{E}-\frac{e_{33}\left(c_{55}^{E}+c_{13}^{E}\right)}{e_{31}+e_{15}}-\frac{e_{15}\left(c_{33}^{E}\varepsilon_{33}^{S}+e_{33}^{2}\right)}{e_{15}\varepsilon_{33}^{S}-e_{33}\varepsilon_{11}^{S}} \\
b_{m4} &= \frac{\left(c_{55}^{E}\varepsilon_{11}^{S}+e_{15}^{2}\right)e_{33}}{e_{15}\varepsilon_{33}^{S}-e_{33}\varepsilon_{11}^{S}}k_m^{2}-\frac{e_{33}\varepsilon_{11}^{S}}{e_{15}\varepsilon_{33}^{S}-e_{33}\varepsilon_{11}^{S}}\omega^2\rho
\end{aligned}
\tag{A. 1}
$$

The coefficients appearing in Eqs. (13) and (14) are defined by

$$
\begin{aligned}
b_2 &= -\frac{a_{m3}b_{m1}b_{m3}}{b_{m4}\left(-a_{m3}b_{m4}+a_{m4}b_{m3}\right)} \\
c_2 &= \frac{a_{m1}b_{m3}^{2}+\left(-a_{m3}b_{m2}-a_{m4}b_{m1}\right)b_{m3}+a_{m3}b_{m4}b_{m1}}{b_{m4}\left(-a_{m3}b_{m4}+a_{m4}b_{m3}\right)} \\
d_2 &= \frac{a_{m2}b_{m3}^{2}+a_{m3}b_{m2}b_{m4}-a_{m4}b_{m2}b_{m3}}{b_{m4}\left(-a_{m3}b_{m4}+a_{m4}b_{m3}\right)} \\
b_3 &= \frac{-a_{m3}b_{m1}b_{m3}c_{m3}+a_{m3}b_{m1}b_{m4}c_{m2}}{b_{m4}\left(-a_{m3}b_{m4}+a_{m4}b_{m3}\right)}
\end{aligned}
\tag{A. 2}
$$

$$c_3 = \frac{\left(a_{m1}b_{m3} - a_{m3}b_{m2}\right)c_{m2}}{a_{m3}b_{m4} - a_{m4}b_{m3}} + \frac{\left(a_{m1}b_{m3}^2 + \left(-a_{m3}b_{m2} - a_{m4}b_{m1}\right)b_{m3} + a_{m3}b_{m4}b_{m1}\right)c_{m3}}{b_{m4}\left(-a_{m3}b_{m4} + a_{m4}b_{m3}\right)}$$

$$d_3 = c_{m1} + \frac{a_{m2}b_{m3}c_{m2}}{a_{m3}b_{m4} - a_{m4}b_{m3}} + \frac{\left(a_{m2}b_{m3}^2 + a_{m3}b_{m2}b_{m4} - a_{m4}b_{m2}b_{m3}\right)c_{m3}}{b_{m4}\left(-a_{m3}b_{m4} + a_{m4}b_{m3}\right)}$$

where

$$c_{m1} = \frac{\left(c_{13}^E + c_{55}^E\right)\varepsilon_{33}^S + \left(e_{31} + e_{15}\right)e_{33}}{\left(e_{15}\varepsilon_{33}^S - e_{33}\varepsilon_{11}^S\right)k_m}$$

$$c_{m2} = \frac{c_{33}^E\varepsilon_{33}^S + e_{33}^2}{k_m^2\left(e_{15}\varepsilon_{33}^S - e_{33}\varepsilon_{11}^S\right)}$$

$$c_{m3} = -\frac{c_{55}^E\varepsilon_{33}^S + e_{15}e_{33}}{e_{15}\varepsilon_{33}^S - e_{33}\varepsilon_{11}^S} + \frac{\omega^2\rho\varepsilon_{33}^S}{\left(e_{15}\varepsilon_{33}^S - e_{33}\varepsilon_{11}^S\right)k_m^2}$$

The coefficients related to the second building block (on the right of Fig. 2(b)) are defined as

$$a_{n1} = \frac{\left(c_{13}^E + c_{55}^E\right)\varepsilon_{11}^S + \left(e_{31} + e_{15}\right)e_{15}}{\left(e_{15}\varepsilon_{33}^S - e_{33}\varepsilon_{11}^S\right)k_n} + \frac{c_{11}^E}{\left(e_{31} + e_{15}\right)k_n}$$

$$a_{n2} = -\frac{c_{55}^E k_n}{e_{31} + e_{15}} + \frac{\rho\omega^2}{\left(e_{31} + e_{15}\right)k_n}$$

$$a_{n3} = -\frac{c_{55}^E\varepsilon_{11}^S + e_{15}^2}{k_n^2\left(e_{15}\varepsilon_{33}^S - e_{33}\varepsilon_{11}^S\right)}$$

$$a_{n4} = \frac{c_{33}^E\varepsilon_{11}^S + e_{15}e_{33}}{e_{15}\varepsilon_{33}^S - e_{33}\varepsilon_{11}^S} + \frac{c_{13}^E + c_{55}^E}{e_{31} + e_{15}} - \frac{\omega^2\rho\varepsilon_{11}^S}{\left(e_{15}\varepsilon_{33}^S - e_{33}\varepsilon_{11}^S\right)k_n^2}$$

$$b_{n1} = -\frac{e_{15}c_{11}^E}{\left(e_{31} + e_{15}\right)k_n}$$

$$b_{n2} = \left(\frac{e_{15}c_{55}^E}{e_{31} + e_{15}} - \frac{\left(c_{13}^E + c_{55}^E\right)e_{15}\varepsilon_{33}^S + \left(e_{31} + e_{15}\right)e_{15}e_{33}}{e_{15}\varepsilon_{33}^S - e_{33}\varepsilon_{11}^S}\right)k_n - \frac{e_{15}\omega^2\rho}{\left(e_{31} + e_{15}\right)k_n} \tag{A. 3}$$

$$b_{n3} = c_{55}^E + \frac{e_{33}\left(c_{55}^E\varepsilon_{11}^S + e_{15}^2\right)}{e_{15}\varepsilon_{33}^S - e_{33}\varepsilon_{11}^S} - \frac{e_{15}\left(c_{13}^E + c_{55}^E\right)}{e_{31} + e_{15}}$$

$$b_{n4} = \frac{\left(c_{33}^E\varepsilon_{33}^S - e_{33}^2\right)e_{15}}{e_{15}\varepsilon_{33}^S - e_{33}\varepsilon_{11}^S}k_n^2 + \frac{e_{15}\varepsilon_{33}^S}{e_{15}\varepsilon_{33}^S - e_{33}\varepsilon_{11}^S}\omega^2\rho$$

$$c_{n1} = \frac{\left(c_{13}^{E} + c_{55}^{E}\right)\varepsilon_{11}^{S} + e_{15}\left(e_{31} + e_{15}\right)}{\left(e_{15}\varepsilon_{33}^{S} - e_{33}\varepsilon_{11}^{S}\right)k_n}$$

$$c_{n2} = -\frac{c_{55}^{E}\varepsilon_{11}^{S} + e_{15}^{2}}{k_n^{2}\left(e_{15}\varepsilon_{33}^{S} - e_{33}\varepsilon_{11}^{S}\right)}$$

$$c_{n3} = \frac{c_{33}^{E}\varepsilon_{11}^{S} + e_{15}e_{33}}{e_{15}\varepsilon_{33}^{S} - e_{33}\varepsilon_{11}^{S}} - \frac{\omega^{2}\rho\varepsilon_{11}^{S}}{\left(e_{15}\varepsilon_{33}^{S} - e_{33}\varepsilon_{11}^{S}\right)k_n^{2}}$$

References

[1] G. Kino, Design of slotted transducer arrays with matched backings, Ultrason. Imaging. 1 (1979) 189–209. https://doi.org/10.1016/0161-7346(79)90016-6.

[2] T. Ikeda, Fundamentals of piezoelectricity, Oxford university press, 1996.

[3] J. Erhart, P. Půlpán, M. Pustka, Piezoelectric Ceramic Resonators, Springer International Publishing, 2017. https://doi.org/10.1007/978-3-319-42481-1.

[4] IEEE Standard on Piezoelectricity, IEEE Trans. Sonics Ultrason. 31 (1984). https://doi.org/10.1109/T-SU.1984.31464.

[5] J.M. Cannata, T.A. Ritter, W.-H. Chen, R.H. Silverman, K.K. Shung, Design of efficient, broadband single-element (20-80 MHz) ultrasonic transducers for medical imaging applications, IEEE Trans. Ultrason. Ferroelectr. Freq. Control. 50 (2003) 1548–1557. https://doi.org/10.1109/tuffc.2003.1251138.

[6] S.T. Lau, H. Li, K.S. Wong, Q.F. Zhou, D. Zhou, Y.C. Li, H.S. Luo, K.K. Shung, J.Y. Dai, Multiple matching scheme for broadband 0.72Pb(Mg1/3Nb2/3)O3-0.28PbTiO3 single crystal phased-array transducer, J. Appl. Phys. 105 (2009) 094908. https://doi.org/10.1063/1.3065476.

[7] C.-M. Wong, Y. Chen, H. Luo, J. Dai, K.-H. Lam, H.L. Chan, Development of a 20-MHz wide-bandwidth PMN-PT single crystal phased-array ultrasound transducer, Ultrasonics. 73 (2017) 181–186. https://doi.org/10.1016/j.ultras.2016.09.012.

[8] M. Brissaud, Characterization of piezoceramics, IEEE Trans. Ultrason. Ferroelectr. Freq. Control. 38 (1991) 603–617. https://doi.org/10.1109/58.108859.

[9] M. Brissaud, Three-dimensional modeling of piezoelectric materials, IEEE Trans. Ultrason. Ferroelectr. Freq. Control. 57 (2010) 2051–2065. https://doi.org/10.1109/TUFFC.2010.1653.

[10] M. Brissaud, Modelling and characterisation of shear modes of rectangular piezoelectric materials, Ferroelectrics. 550 (2019) 12–35. https://doi.org/10.1080/00150193.2019.1652494.

[11] N. Lamberti, M. Pappalardo, A general approximated two-dimensional model for piezoelectric array elements, IEEE Trans. Ultrason. Ferroelectr. Freq. Control. 42 (1995) 243–252. https://doi.org/10.1109/58.365238.

[12] A. Iula, N. Lamberti, M. Pappalardo, An approximated 3-D model of cylinder-shaped piezoceramic elements for transducer design, IEEE Trans. Ultrason. Ferroelectr. Freq. Control. 45 (1998) 1056–1064. https://doi.org/10.1109/58.710588.

[13] H.F. Tiersten, Linear Piezoelectric Plate Vibrations, 1969.

https://doi.org/10.1007/978-1-4899-6453-3.
[14] M. Kim, J. Kim, W. Cao, Electromechanical coupling coefficient of an ultrasonic array element, J. Appl. Phys. 99 (2006) 074102. https://doi.org/10.1063/1.2180487.
[15] P.C.Y. Lee, J.D. Yu, W.S. Lin, A new two-dimensional theory for vibrations of piezoelectric crystal plates with electroded faces, J. Appl. Phys. 83 (1998) 1213–1223. https://doi.org/10.1063/1.366818.
[16] R. Huang, P.C.Y. Lee, W.-S. Lin, J.-D. Yu, Extensional, thickness-stretch and symmetric thickness-shear vibrations of piezoceramic disks, IEEE Trans. Ultrason. Ferroelectr. Freq. Control. 49 (2002) 1507–1515. https://doi.org/10.1109/tuffc.2002.1049732.
[17] N. Li, B. Wang, Z. Qian, I. Kuznetsova, T. Ma, Two-Dimensional Plate Theory for the Analysis of Coupling Vibrations in Shear Mode FBARs, IEEE Trans. Ultrason. Ferroelectr. Freq. Control. 67 (2020) 1897–1908. https://doi.org/10.1109/tuffc.2020.2992287.
[18] E. Giebe, E. Blechschmidt, Experimentelle und theoretische Untersuchungen über Dehnungseigenschwingungen von Stäben und Rohren [Experimental and theoretical investigations on natural elongation vibrations of rods and tubes], Ann. Phys. 410 (1933) 417–456. https://doi.org/10.1002/andp.19334100406.
[19] D.J. Gorman, Free vibration analysis of the completely free rectangular plate by the method of superposition, J. Sound Vib. 57 (1978) 437–447. https://doi.org/10.1016/0022-460x(78)90322-x.
[20] W. Ritz, Über eine neue Methode zur Lösung gewisser Variationsprobleme der mathematischen Physik [A new method for solving certain variation problems in mathematical physics]., J. Für Reine Angew. Math. Crelles J. 1909 (1909) 1–61. https://doi.org/10.1515/crll.1909.135.1.
[21] C. Rajalingham, R. Bhat, G. Xistris, Vibration of rectangular plates using plate characteristic functions as shape functions in the Rayleigh–Ritz method, J. Sound Vib. 193 (1996) 497–509. https://doi.org/10.1006/jsvi.1996.0298.
[22] S. Bashmal, R. Bhat, S. Rakheja, In-plane free vibration of circular annular disks, J. Sound Vib. 322 (2009) 216–226. https://doi.org/10.1016/j.jsv.2008.11.024.
[23] Sh. Hosseini Hashemi, H. Kalbasi, H. Rokni Damavandi Taher, Free vibration analysis of piezoelectric coupled annular plates with variable thickness, Appl. Math. Model. 35 (2011) 3527–3540. https://doi.org/10.1016/j.apm.2011.01.003.
[24] P. Laura, R. Duran, A note on forced vibrations of a clamped rectangular plate, J. Sound Vib. 42 (1975) 129–135. https://doi.org/10.1016/0022-460X(75)90307-7.
[25] K.Y. Dai, G.R. Liu, X. Han, K.M. Lim, Thermomechanical analysis of functionally graded material (FGM) plates using element-free Galerkin method, Comput. Struct. 83 (2005) 1487–1502. https://doi.org/10.1016/j.compstruc.2004.09.020.
[26] S. Jayasinghe, S.M. Hashemi, A Dynamic Coefficient Matrix Method for the Free Vibration of Thin Rectangular Isotropic Plates, Shock Vib. 2018 (2018) 1–8. https://doi.org/10.1155/2018/1071830.
[27] S. Yu, X. Yin, A generalized superposition method for accurate free vibration analysis of rectangular plates and assemblies, J. Acoust. Soc. Am. 145 (2019) 185–203. https://doi.org/10.1121/1.5085778.
[28] D. Tang, F. Pang, L. Li, X. Yao, A semi-analytical solution for in-plane free waves analysis of rectangular thin plates with general elastic support boundary

conditions, Int. J. Mech. Sci. 168 (2020) 105290. https://doi.org/10.1016/j.ijmecsci.2019.105290.
[29] D.J. Gorman, Free in-plane vibration analysis of rectangular plates by the method of superposition, J. Sound Vib. 272 (2004) 831–851. https://doi.org/10.1016/S0022-460X(03)00421-8.
[30] D.J. Gorman, Accurate in-plane free vibration analysis of rectangular orthotropic plates, J. Sound Vib. 323 (2009) 426–443. https://doi.org/10.1016/j.jsv.2008.12.021.
[31] D.J. Gorman, S.D. Yu, A review of the superposition method for computing free vibration eigenvalues of elastic structures, Comput. Struct. 104–105 (2012) 27–37. https://doi.org/10.1016/j.compstruc.2012.02.018.
[32] D. Kim, M. Kim, K. Kang, K. Son, S. Lee, Coupled vibration analysis for a piezoelectric array element using superposition method, in: 2013 IEEE Int. Ultrason. Symp. IUS, 2013: pp. 2179–2182. https://doi.org/10.1109/ULTSYM.2013.0557.
[33] D. Royer, E. Dieulesaint, Elastic waves in solids I: Free and guided propagation, Springer Science & Business Media, 1999.
[34] M. Abramowitz, I.A. Stegun, Handbook of mathematical functions with formulas, graphs, and mathematical tables, US Government printing office, 1948.
[35] Cubic formula, (2002). https://mathworld.wolfram.com/CubicFormula.html (accessed September 15, 2020).
[36] S. Kevorkian, M. Pascal, An accurate method for free vibration analysis of structures with application to plates, J. Sound Vib. 246 (2001) 795–814.
[37] G.T. Stranford, T. Vencill, D. Williams, B. Johnson, L. Gutierrez, Piezoelectric ceramics in ultrasound, in: 2014 IEEE Int. Ultrason. Symp., 2014: pp. 897–902. https://doi.org/10.1109/ULTSYM.2014.0220.
[38] D.J. Powell, G.L. Wojcik, C.S. Desilets, T.R. Gururaja, K. Guggenberger, S. Sherrit, B.K. Mukherjee, Incremental model-build-test validation exercise for a 1-D biomedical ultrasonic imaging array, in: 1997 IEEE Ultrason. Symp. Proc., 1997: pp. 1669–1674. https://doi.org/10.1109/ULTSYM.1997.663316.
[39] PZT Materials Complete Properties, (2018). https://www.ctscorp.com/wp-content/uploads/CTS_-PZT-Materials_Complete-Properties_20180829.pdf (accessed September 15, 2020).